Faraday Discussions

Cite this: *Faraday Discuss.*, 2015, **180**, 283

PAPER

The influence of hydrogen peroxide and hydrogen on the corrosion of simulated spent nuclear fuel

Mayuri Razdan and David W. Shoesmith*

Received 15th November 2014, Accepted 16th January 2015
DOI: 10.1039/c4fd00221k

The synergistic influence between H_2O_2 and H_2 on the corrosion of SIMFUEL (simulated spent nuclear fuel) has been studied in solutions with and without added HCO_3^-/CO_3^{2-}. The response of the surface to increasing concentrations of added H_2O_2 was monitored by measuring the corrosion potential in either Ar or Ar/H_2-purged solutions. Using X-ray photoelectron spectroscopy it was shown that the extent of surface oxidation (U^V + U^{VI} content) was directly related to the corrosion potential. Variations in corrosion potential with time, redox conditions, HCO_3^-/CO_3^{2-} concentration, and convective conditions showed that surface oxidation induced by H_2O_2 could be reversed by reaction with H_2, the latter reaction occurring dominantly on the noble metal particles in the SIMFUEL. For sufficiently large H_2O_2 concentrations, the influence of H_2 was overwhelmed and irreversible oxidation of the surface to U^{VI} occurred. Subsequently, corrosion was controlled by the chemical dissolution rate of this U^{VI} layer.

1. Introduction

The Canadian concept to ensure the long term safe disposal of used nuclear fuel is based on multiple barriers: the used fuel bundles, a durable carbon steel container with an outer Cu shell, a clay buffer which seals around the container, and a deep stable geologic environment.[1] Based on this approach it can be calculated that long term containment should be achieved,[2] but it is judicious to assume container failure leading to the exposure of the fuel to groundwater will occur. On failure, the groundwater entering the container would be anoxic since oxidants, mainly dissolved O_2, trapped in the repository on sealing, will be rapidly consumed by minerals (*e.g.*, iron oxides) and biochemical reactions in the surrounding clays, and by corrosion of the copper container.[3] However, radiolysis of the groundwater caused by the radioactivity in the fuel can produce oxidizing conditions at the fuel surface, leading to an increase in solubility of the fuel by

Department of Chemistry and Surface Science Western, University of Western Ontario, London, ON, N6A 5B7, Canada. E-mail: dwshoesm@uwo.ca; Tel: +1-519-661-2111 ext. 86366

many orders of magnitude.[4,5] This could lead to fuel corrosion and the release of radionuclides would be expected.

The fuel corrosion process involves a sequence of oxidation, dissolution, and possibly, corrosion product deposition reactions,

$$U^{IV}O_2 \rightarrow U^{IV}_{1-2x}U^{V}_{2x}O_{2+x} \rightarrow U^{VI}O_2^{2+} \rightarrow U^{VI}O_3 \cdot yH_2O \quad (1)$$

where $U^{IV}_{1-2x}U^{V}_{2x}O_{2+x}$ is a thin intermediate oxide layer[6] and $U^{VI}O_3 \cdot yH_2O$ is an outer surface layer on the $U^{IV}O_2$ surface. Since, the anticipated ground water pH will be between 6 and 9 (when U^{VI} is at a solubility minimum), corrosion product films would be expected to form and to influence the corrosion rate.[7–9]

In Canadian groundwater, the key constituent likely to influence fuel dissolution is HCO_3^-/CO_3^{2-} (10^{-4} to 10^{-3} mol L^{-1}),[10] which increases the solubility of $U^{VI}O_2^{2+}$ by complexation[11] and buffers the pH. In the presence of HCO_3^-/CO_3^{2-}, the rate of oxidative dissolution is expected to increase, since the formation of $U^{VI}O_3 \cdot yH_2O$ would be retarded, and the overall corrosion reaction would become limited by the rate of surface oxidation (to $U^{IV}_{1-2x}U^{V}_{2x}O_{2+x}$). For $[CO_3^{2-}] \geq 10^{-3}$ mol L^{-1}, both electrochemical[6,12,13] and chemical studies[14–16] show not only is $U^{VI}O_3 \cdot yH_2O$ formation prevented but the formation of the underlying $U^{IV}_{1-2x}U^{V}_{2x}O_{2+x}$ layer is retarded[14,15] and oxidative dissolution becomes strongly promoted.[13]

In a reactor, irradiation leads to key changes in the composition and properties of the $U^{IV}O_2$ matrix.[17–19] Of these possible changes two are particularly important from a corrosion perspective: (i) rare earth (RE^{III}) doping of the $U^{IV}O_2$ matrix, which will significantly increase its conductivity, and (ii) the segregation of some fission products into noble metal (ε) particles.[20,21] This dispersion of noble metal particles throughout an electrically conducting matrix introduces the possibility of separated, and galvanically-coupled anodes and cathodes which would be expected to significantly influence fuel corrosion in the presence of radiolytic oxidants (particularly H_2O_2).[22,23]

Within a failed and groundwater-flooded container two corrosion fronts exist, Fig. 1, one on the fuel surface and a second on the inner surface of the carbon steel vessel where steel corrosion is sustained by reaction with water to produce Fe^{2+} and H_2:

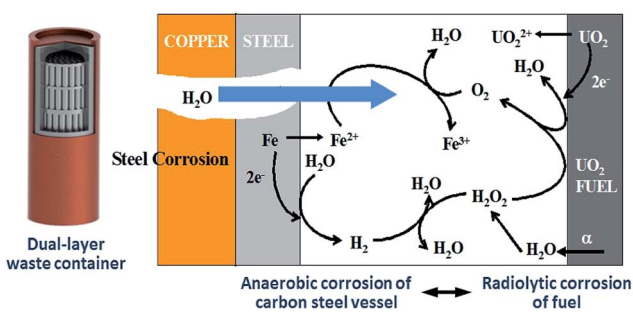

Fig. 1 Schematic showing a cut-away of a dual-walled waste container and the two corrosion fronts that would exist within the container after failure and flooding with groundwater.

$$Fe + 2H_2O \rightarrow Fe^{2+} + H_2 + 2OH^- \quad (2)$$

$$3Fe + 4H_2O \rightarrow Fe_3O_4 + 4H_2 \quad (3)$$

This introduces the possibility that the products of steel corrosion will scavenge the radiolytic oxidants (primarily H_2O_2) responsible for fuel corrosion. Many studies on the influence of Fe and Fe corrosion products on fuel corrosion have been published (ref. 24 and references therein) and inevitably show that the presence of Fe suppresses fuel corrosion and radionuclide release.

However, it is not possible to separate the redox controlling influences of Fe^{2+} and H_2 from steel corrosion and considerable effort has been expended in studying them separately. The influences of Fe^{2+} and Fe_3O_4 on fuel corrosion have been studied extensively[22] and Jonsson *et al.*[25] calculated that the consumption of H_2O_2 *via* the homogeneous Fenton reaction could suppress $U^{IV}O_2$ corrosion inside a failed container by a factor of >40.

$$Fe^{2+} + H_2O_2 \rightarrow Fe^{3+} + OH^{\bullet} + OH^- \quad (4)$$

$$Fe^{2+} + OH^{\bullet} \rightarrow Fe^{3+} + OH^- \quad (5)$$

There is now a considerable amount of evidence to show that H_2 has a more significant effect on the suppression of fuel corrosion than Fe^{2+}, primarily by H_2 oxidation on noble metal (ε) particles galvanically coupled to the UO_2 matrix.[24,26,27]

The overall rate of fuel corrosion will be determined by the relative rates of a series of possible reactions on the fuel surface. To determine the overall influence of these many reactions we have developed a model to determine the influence of steel corrosion products on the alpha (α) radiolytic corrosion of spent nuclear fuel within a failed waste container.[28–30] The key reactions incorporated in this model are illustrated in Fig. 2 and include: (1) a complete reaction set for the α-radiolysis

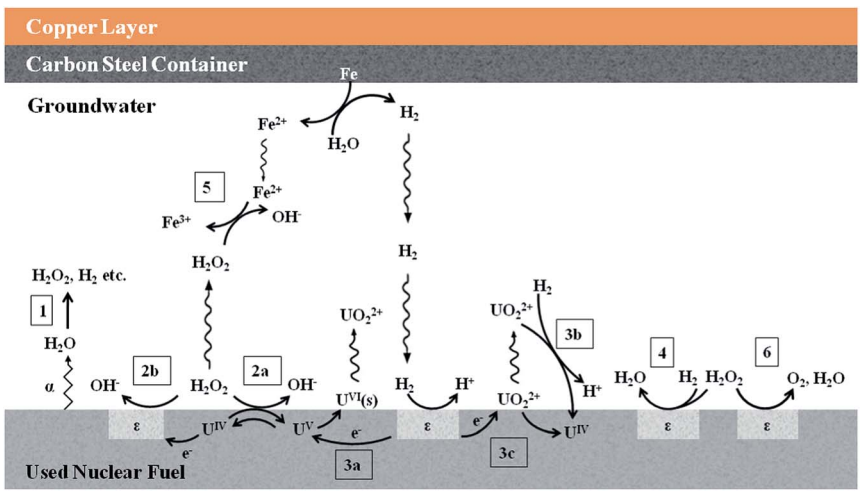

Fig. 2 Reactions involved in the model for the α-radiolytic corrosion of spent nuclear fuel inside a failed nuclear waste container.[29]

of H_2O including the generation of, and the interactions between, the radiolysis products; (2) the oxidative dissolution (corrosion) of $U^{IV}O_2$ supported by H_2O_2 reduction on both the $U^{IV}O_2$ surface (2a) and the noble metal (ε) particles (2b); (3) the reduction of oxidized surface species (U^V/U^{VI}) by H_2 oxidation on noble metal (ε) particles (3a) and of dissolved $U^{VI}O_2^{2+}$ either by reaction with H_2 in solution (3b) or with H_2 catalyzed on the fuel surface (3c); (4) the reaction of H_2O_2 with H_2 catalyzed by noble metal (ε) particles; (5) the scavenging of H_2O_2 by the Fenton reaction; and (6) the decomposition of H_2O_2 to O_2 and H_2O.

One key, but not comprehensively understood, feature of this model is the role the chemical state of the UO_2 surface plays in determining the fuel reactivity in H_2O_2/H_2-containing solutions; *i.e.*, reactions (2a) and (2b). Here, we investigate these reactions in solutions containing various relative concentrations of H_2O_2 and H_2 on 1.5 at% SIMFUEL in solutions with and without added HCO_3^-/CO_3^{2-}.

2. Experimental

2.1 Electrode materials

Experiments were conducted on a 1.5 at% SIMFUEL fabricated by Canadian Nuclear Laboratories Limited (Chalk River, Ontario). SIMFUEL is a simulated chemical fuel, produced by doping UO_2 with eleven stable elements (Y, La, Ce, Mo, Sr, Ba, Rh, Zr, Ru, Nd, and Pd) in the proportions required to simulate spent fuel with a specific in-reactor burn up. The noble metal dopants (Mo, Rh, Pd, and Ru) are unstable as oxides and separate during fabrication to form noble metal (ε) particles, uniformly distributed in the UO_2 matrix.[31] The microstructure of the material is typical of CANDU fuel with grains 8–15 μm in size and a density ~97% of the theoretical value. Secondary ion mass spectrometry confirms the presence of noble metal particles.[24] The electrodes used were ~2 mm thick and 1.2 cm in diameter and were prepared from pellets using a procedure described in detail elsewhere.[32]

2.2 Electrochemical cell and equipment

A standard three compartment glass cell was employed in all experiments. The working electrode was a 1.5 at% SIMFUEL disc, set in resin to expose only one flat face to the solution. A Luggin capillary was used to minimize any ohmic potential drop between the working and reference electrodes. The reference electrode was a commercially available saturated calomel electrode (SCE, Fischer Scientific). The counter electrode was a Pt foil, with a surface area of ~6 cm^2, spot-welded to a Pt wire (99.9% purity, Alfa Aesar). All potentials were measured, and are quoted, against the SCE scale. The cell was housed in a grounded Faraday cage to minimize interference from external sources of noise. A Solartron Model 1287 potentiostat was used to control experiments and record electrochemical data. Corrware™ software (supplied by Scribner and Associates) was used to control instrumentation.

2.3 Electrode polishing and solution preparation

Electrodes were manually polished (wet) with 1200 grit SiC paper and polishing residue was removed by sonication with deionized water before each experiment. Any air-formed oxides were reduced at a cathodic potential of −1500 mV (*vs.* SCE)

applied for 5 min before each experiment. On removal from the electrochemical cell, the electrode was rinsed with deionized water and air dried prior to analysis by X-ray photoelectron spectroscopy (XPS).

Solutions were prepared using distilled deionized water purified using a NANOpure Diamond UV ultrapure water system from Barnstead International which removes organic and inorganic impurities ($\rho = 18.2$ MΩ cm). Experiments were carried out in a 0.1 mol L^{-1} NaCl (Caledon, >99%) solution purged with UHP Ar or 5% H_2/95% Ar ($[H_2] \sim 10^{-4}$ mol L^{-1}) gas (Praxair) with and without added HCO_3^-/CO_3^{2-}. Solutions were purged for a minimum of an hour prior to the start of an experiment to minimize dissolved O_2 levels. The 5×10^{-2} mol L^{-1} HCO_3^-/CO_3^{2-} solution was prepared with Na_2CO_3 and $NaHCO_3$ (Caledon, >99%) and the pH adjusted to ~9 (when required) using NaOH and an Orion Model 720A pH meter. Stock solutions of H_2O_2 were prepared using an appropriate amount of 3% w/v solution (Fisher Scientific) and the desired cell concentration (10^{-8} to 10^{-5} mol L^{-1}) was achieved by adding the required amount of this solution into the electrolyte. The H_2O_2 concentration used was determined by ultra-violet/visible spectrophotometry.

2.4 Experimental procedure

The corrosion potential (E_{CORR}) measurements were performed at ambient temperature. E_{CORR} was monitored continuously as the $[H_2O_2]$ was periodically increased. When required the solution was stirred using an external magnetic stirrer.

2.5 UV-vis spectrophotometry

Hydrogen peroxide concentrations were determined spectrophotometrically using a BioLogic Science Instruments MOS UV-vis spectrophotometer. The Ghormley tri-iodide method was employed with ammonium molybdate used to catalyze the oxidation of I^- to I_3^- by H_2O_2. The I_3^- produced has a maximum absorption at 350 nm with a molar extinction coefficient of 25 500 mol L^{-1} cm^{-1}.[33]

2.6 XPS surface analysis

A Kratos Axis Ultra spectrometer was used to record XPS spectra. Spectra were excited using an Al K_α (15 mA, 14 kV) monochromatic high energy ($h\nu = 1486.6$ eV) radiation source. The spectrometer work function was set to give a value of 83.96 eV for the binding energy (BE) of the Au $4f_{7/2}$ line of metallic Au. The instrument was calibrated to give a BE of 932.62 eV for the Cu $2p_{3/2}$ line of Cu metal. Survey spectra were collected over the energy range from 0 to 1100 eV with an X-ray spot size of ~300 to 700 μm at a pass energy of 160 eV. Charge neutralization was used on all specimens. The C 1s peak at 285.0 eV was used as a standard to correct for surface charging.

All spectra were analyzed using CasaXPS software (version 2.3.14) and involved a 50% Gaussian and 50% Lorentzian fitting routine with a Shirley background correction. The procedure used to deconvolute the U 4f spectra into contributions from U^{IV}, U^V, and U^{VI} has been described elsewhere.[33–36] The resolved components in both spin–orbit split peaks and the associated satellite structures were used to calculate the proportion of each oxidation state in the surface. The positions and

shapes of the satellite structures were used to confirm the validity of the deconvolution of the U 4f peaks.

3. Results and discussion

Fig. 3 shows a series of measurements of E_{CORR} in stirred Ar-purged solutions with and without added HCO_3^-/CO_3^{2-}. Prior to the first H_2O_2 addition, E_{CORR} was allowed to stabilize, and each subsequent H_2O_2 addition was made only after E_{CORR} achieved a steady-state value at the existing $[H_2O_2]$.

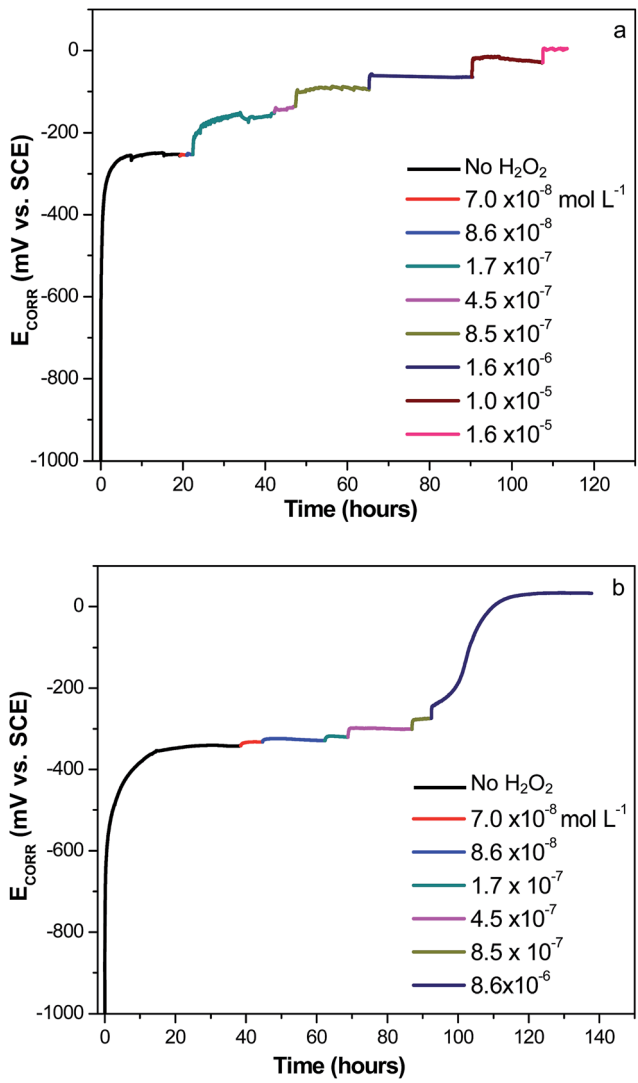

Fig. 3 E_{CORR} as a function of time for different $[H_2O_2]$ measured on a 1.5 at% SIMFUEL electrode in stirred Ar-purged 0.1 mol L^{-1} NaCl solution (pH ~ 9) (a) without and (b) with 0.05 mol L^{-1} HCO_3^-/CO_3^{2-}.

For the solution containing no HCO_3^-/CO_3^{2-}, the addition of $<10^{-7}$ mol L^{-1} H_2O_2 had no observable influence on E_{CORR}, Fig. 3(a). Subsequent additions to higher $[H_2O_2]$ led to increases in E_{CORR} to higher steady-state values, which depended on $[H_2O_2]$. This dependence of E_{CORR} on $[H_2O_2]$ suggests the $U^{IV}O_2$ surface becomes progressively more oxidized as the $[H_2O_2]$ increases. The lack of sensitivity of E_{CORR} to $[H_2O_2]$ below 10^{-7} mol L^{-1} is in contrast to previous experiments conducted at 60 °C,[27] in which E_{CORR} responded to H_2O_2 additions in the concentration range 10^{-11} to 10^{-10} mol L^{-1}.

Previous studies[6,27,37] suggest that the extent of oxidation of the surface (as defined by x in $U^{IV}_{1-2x}U^{V}_{2x}O_{2+x}$) is proportional to the E_{CORR} over the potential range −400 mV to ~0 mV in the absence of HCO_3^-/CO_3^{2-}.

For the experiments conducted in the solution containing 0.05 mol L^{-1} HCO_3^-/CO_3^{2-}, Fig. 3(b), E_{CORR} responded much less markedly to H_2O_2 additions over the concentration range 7×10^{-8} mol L^{-1} to 8.5×10^{-7} mol L^{-1}, changing only marginally. After the final addition of 8.6×10^{-6} mol L^{-1}, E_{CORR} underwent a major transition over a period of ~20 hours to a value >0 mV, effectively the same value achieved in the absence of HCO_3^-/CO_3^{2-} at higher $[H_2O_2]$, Fig. 3(a). This marked increase in E_{CORR} suggests a slow irreversible oxidation of the $U^{IV}O_2$ surface. The lack of response of E_{CORR} to $[H_2O_2]$ at the low concentrations suggests either the UO_2 is not oxidized or, more likely, oxidized to U^{VI} (as $U^{VI}O_2^{2+}$) and subsequently complexed by carbonate ($U^{VI}O_2(CO_3)_x^{(2-x)+}$)

$$U^{VI}O_3 \cdot yH_2O + 2HCO_3^- \rightarrow U^{VI}O_2(CO_3)_2^{2-} + (y + 1)H_2O \quad (6)$$

and dissolved, thereby, maintaining the electrode surface unoxidized.[22]

Previous experiments showed that E_{CORR} became independent of H_2O_2 at $[H_2O_2] \geq 10^{-5}$ mol L^{-1}, irrespective of whether HCO_3^-/CO_3^{2-} was present or not.[38] Wren *et al.*[39] observed a similar trend from a dependence on $[H_2O_2]$ (produced by α-radiolysis) at low values of $[H_2O_2]$ to independence at high concentrations. This independence was attributed to the formation of an insulating U^{VI} surface layer (possibly $U^{VI}O_3 \cdot yH_2O$), which lead to a condition of redox buffering, with both $U^{IV}O_2$ corrosion and H_2O_2 decomposition occurring at rates determined by the rate of release of U^{VI} to solution to expose the underlying conductive $U^{IV}_{1-2x}U^{V}_{2x}O_{2+x}$. This mechanism has recently been confirmed[40] and the influence of HCO_3^-/CO_3^{2-} demonstrated.[41]

The results in Fig. 3 suggest the surface in both the present experiments is oxidized to U^{VI} at the final $[H_2O_2]$. Of more interest in the present study is the potential range over which the electrode surface is oxidized to $U^{IV}_{1-2x}U^{V}_{2x}O_{2+x}$ but not covered by a passive layer of insulating U^{VI} (as $U^{VI}O_3 \cdot yH_2O$). In the stoichiometric form, $U^{IV}O_2$ is a Mott–Hubbard insulator with a filled narrow U 5f band, located in the ~5 eV gap between the filled valence band and the empty conduction band. However, the introduction of surface non-stoichiometry, in the form of oxygen interstitial ions (O_I^{II}) accompanied by the creation of U^V atoms to maintain charge balance, creates holes in the 5f band and an increase in electrical conductivity. Under these conditions the surface should be able to sustain cathodic reactions, may be catalytic, and could be susceptible to corrosion.

Fig. 4 shows the response of E_{CORR} to H_2O_2 additions in stirred solutions purged with 5% H_2/Ar with and without added HCO_3^-/CO_3^{2-}. The initial E_{CORR} value recorded in the solution containing no HCO_3^-/CO_3^{2-} is significantly lower

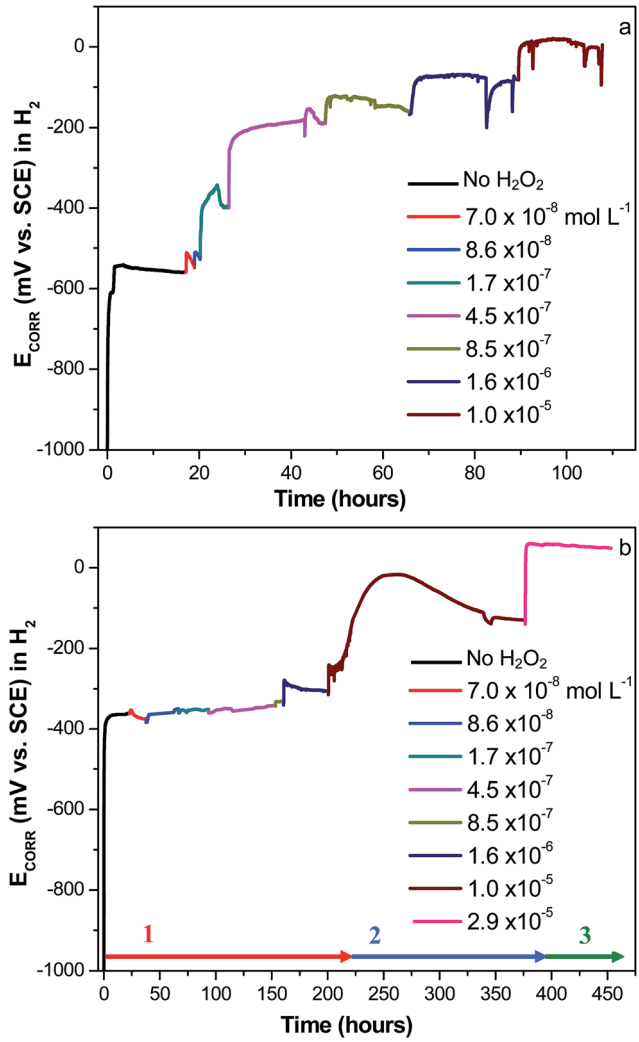

Fig. 4 E_{CORR} as a function of time for different $[H_2O_2]$ measured on a 1.5 at% SIMFUEL electrode in stirred 5% H_2/95% Ar-purged 0.1 mol L^{-1} NaCl (pH ~ 9) (a) without and (b) with 0.05 mol L^{-1} HCO_3^-/CO_3^{2-}.

than that observed in the Ar-purged solution (Fig. 3(a)). This is expected when dissolved H_2 is present,[24,27] since H_2 oxidation on the noble metal particles has been shown to retard oxidation of the galvanically-coupled RE^{III}-doped UO_2 matrix.[26,42] In the absence of HCO_3^-/CO_3^{2-}, Fig. 4(a), E_{CORR} responds in a similar manner to that observed in Ar-purged solutions, but steady-state values at individual $[H_2O_2]$ were not so readily achieved. For $[H_2O_2] \leq 10^{-7}$ mol L^{-1}, E_{CORR} initially increases on the addition of H_2O_2 before decreasing again. Previous experiments at a higher temperature (60 °C)[27] indicated that such a behavior in E_{CORR} can be attributed to the consumption of H_2O_2 by reaction with dissolved H_2.

A number of possible pathways for such a reaction were proposed. One possible pathway involves the production of $OH^{\bullet}$ radicals by H_2O_2 decomposition on noble metal (ε) particles

$$H_2O_2 \rightarrow 2(OH^{\bullet})_{\varepsilon} \quad (7)$$

followed by their scavenging by reaction with dissolved H_2

$$(OH^{\bullet})_{\varepsilon} + H_2 \rightarrow H^+ + H_2O \quad (8)$$

as illustrated in Fig. 5(a).

Alternatively, H_2 oxidation on noble metal (ε) particles

$$H_2 \rightarrow 2H^{\bullet} \quad (9)$$

$$2H^{\bullet} \rightarrow 2H^+ + 2e^- \quad (10)$$

could galvanically couple to H_2O_2 oxidation on the fuel surface

$$H_2O_2 \rightarrow 2(OH^{\bullet})_{UO_2} \quad (11)$$

$$2(OH^{\bullet})_{UO_2} + 2e^- \rightarrow 2OH^- \quad (12)$$

preventing the reaction of the $OH^{\bullet}$ radicals with UO_2 to cause corrosion, as illustrated schematically in Fig. 5(b). Since the number density of noble metal particles is low in the SIMFUEL used in our experiment, the second reaction pathway is intuitively more likely.[27]

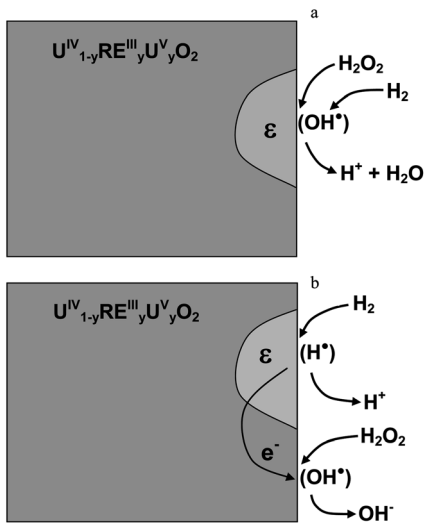

Fig. 5 Schematic illustrating the possible reaction pathways for the consumption of H_2O_2 by reaction with H_2 on a galvanically-coupled 1.5 at% SIMFUEL surface in the presence of H_2O_2 and H_2: (a) on noble metal (ε) particles; (b) by H_2 oxidation on ε-particles galvanically coupled to the oxide matrix.

At 60 °C, it was demonstrated that a concentration ratio, $[H_2]/[H_2O_2]$ of $\geq 10^6$ was required to completely inhibit oxidation of the UO_2 surface by H_2O_2. In the present experiments, E_{CORR} was not followed for a sufficient period of time at these low $[H_2O_2]$ to determine whether the value measured prior to H_2O_2 addition would eventually be re-established; *i.e.*, whether a dissolved $[H_2] \sim 10^{-4}$ mol L^{-1} was sufficient to inhibit surface oxidation for $[H_2O_2] \leq 10^{-7}$ mol L^{-1}.

Further increases in $[H_2O_2]$ in the absence of HCO_3^-/CO_3^{2-}, Fig. 4(a), lead to increased E_{CORR} values, which are maintained for substantially longer periods, although even at $[H_2O_2] \sim 8.5 \times 10^{-7}$ mol L^{-1} there is some indication that E_{CORR} is slowly decreasing, suggesting the catalyzed consumption of H_2O_2 by reaction with H_2 and a decrease in extent of oxidation of the UO_2 surface. At a $[H_2O_2]$ in the range of 10^{-6} to 10^{-5} mol L^{-1}, E_{CORR} apparently achieves a steady-state but is sensitive to convection. Short pauses in stirring (seen in Fig. 4(a) as negative potential excursions) lead to a decrease, and its re-establishment to an increase, in E_{CORR} to the original value. Two examples of such transients due to the interruption of convection are shown in Fig. 6.

The decrease in E_{CORR} occurs on the time scale of a few minutes consistent with the transport controlled depletion of H_2O_2 at the UO_2 surface. The recovery in E_{CORR} on restablishing a convective flow is considerably slower. Additionally, the comparison of the two transients shows the rate of recovery may depend on the value to which E_{CORR} is allowed to decay prior to the re-establishment of the convective flow conditions. The re-establishment of convective conditions would be expected to rapidly restore the surface $[H_2O_2]$, suggesting that the slow response in E_{CORR} must be related to slow changes in the chemical state of the $U^{IV}O_2$ surface.

A similar sensitivity to the local $[H_2O_2]$ was observed previously in thin-layer experiments, in which the local concentration of H_2O_2 was generated by α-radiolysis.[39] Since these previous experiments were conducted on UO_2, not SIMFUEL, this sensitivity to local $[H_2O_2]$ can be considered a feature of the UO_2 surface and not dependent on the presence of noble metal particles.

In the presence of HCO_3^-/CO_3^{2-}, as observed with Ar-purging (Fig. 3(b)), E_{CORR} does not increase significantly with H_2O_2 additions up to $[H_2O_2] \leq 10^{-6}$ mol L^{-1},

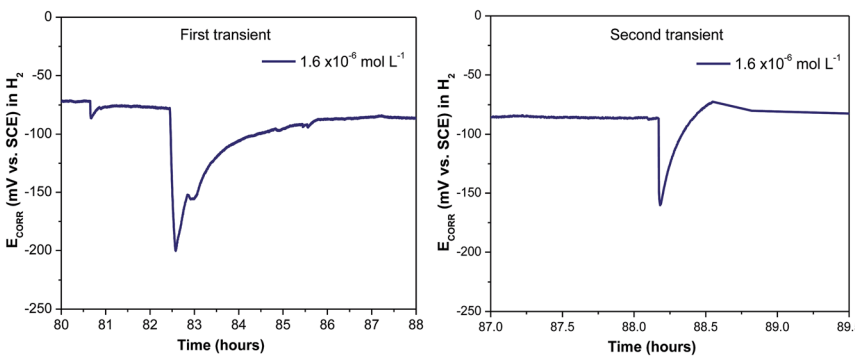

Fig. 6 E_{CORR} as a function of time for $[H_2O_2] \sim 1.6 \times 10^{-6}$ mol L^{-1} obtained on a 1.5 at% SIMFUEL electrode in 5% H_2/95% Ar-purged 0.1 mol L^{-1} NaCl (pH ~ 9) without HCO_3^-/CO_3^{2-}, showing the influence of short periods when stirring was ceased (E_{CORR} decreases) and then re-established (E_{CORR} increases).

Fig. 4(b). At higher $[H_2O_2]$, E_{CORR} begins to increase, indicating irreversible oxidation of the $U^{IV}O_2$ surface. However, the time-dependent behaviour at $[H_2O_2] = 10^{-5}$ mol L^{-1} can be contrasted to that observed in Ar-purged solution at approximately the same $[H_2O_2]$ (8.6×10^{-6} mol L^{-1}), Fig. 3(b). In the Ar-purged solution, E_{CORR} rises steadily to a steady-state value >0 mV, indicating irreversible oxidation of the $U^{IV}O_2$ surface, possibly to the U^{VI} state. By contrast, in H_2/Ar-purged solution, E_{CORR} initially increases before eventually decreasing towards a much lower steady-state value (<−100 mV). This transient behaviour suggests that while the added H_2O_2 may initially oxidize the surface, its consumption by reaction with H_2 eventually leads to a decrease in the extent of the surface oxidation.

The very slow nature of the E_{CORR} response suggests a competition between the H_2O_2 driven oxidation of the surface and its reversal by galvanically-coupled (on ε-particles) or direct (on the UO_{2+x} surface) H_2 oxidation. Since the inventory of H_2O_2 is limited by the amount added while the $[H_2]$ is maintained by continuous purging, the reversal in E_{CORR} from positive-going to negative-going may reflect the decrease in $[H_2O_2]$ as it is consumed by these reactions. Such transient behavior was much more marked at 60 °C even at considerably lower $[H_2O_2]$.[27] Similar transient behavior was observed at 60 °C on a SIMFUEL not containing noble metal (ε) particles, consistent with the α-radiolysis experiments,[39] indicating that the reversible oxidation of the $U^{IV}O_2$ surface is involved and not simply the consumption of H_2O_2 by H_2 catalyzed by noble metal particles.

Fig. 7 summarizes the final steady-state E_{CORR} values as a function of $[H_2O_2]$ for these two sets of experiments. In the absence of HCO_3^-/CO_3^{2-} an influence of H_2 on E_{CORR} becomes significant for $[H_2O_2] \leq 10^{-6}$ mol L^{-1}. In the solution containing HCO_3^-/CO_3^{2-}, the influence of HCO_3^-/CO_3^{2-} is clear by comparison to the values when no carbonate is present. The influence of H_2 is also clear, as E_{CORR} values are consistently lower when H_2 is present.

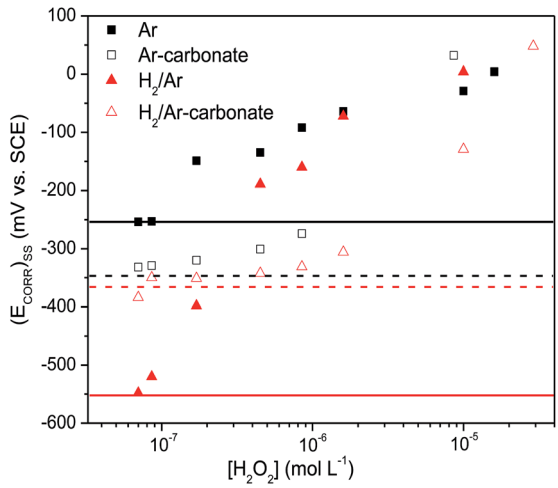

Fig. 7 Comparison of steady-state E_{CORR} values for various $[H_2O_2]$ obtained from Fig. 3 and 4 in Ar and 5% H_2/95% Ar-purged with and without HCO_3^-/CO_3^{2-} in solution. The full and dashed horizontal lines show the E_{CORR} values recorded in the individual experiments prior to the addition of H_2O_2.

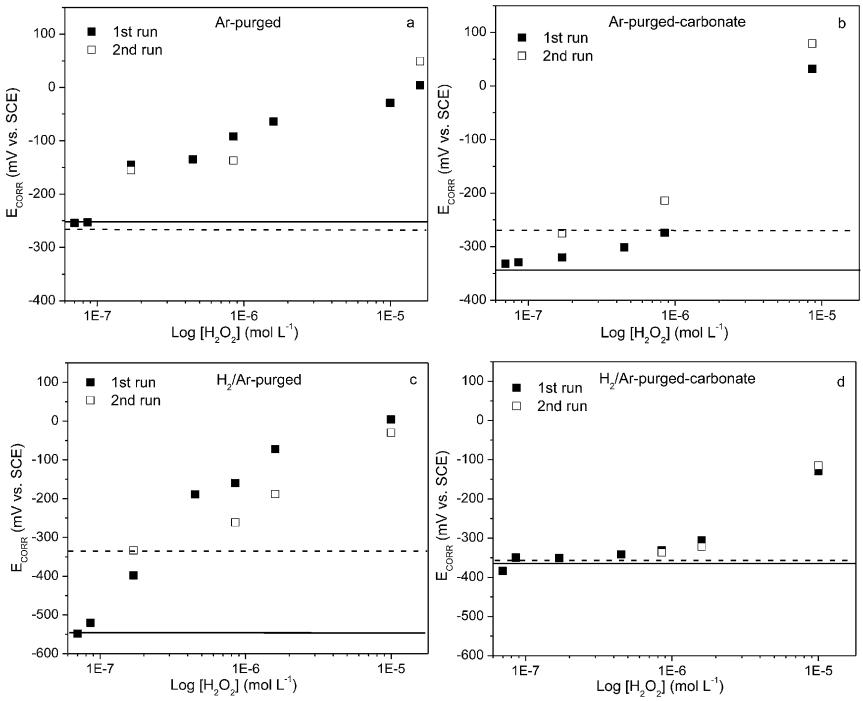

Fig. 8 Comparison of steady-state E_{CORR} values measured on a 1.5 at% SIMFUEL electrode for various $[H_2O_2]$ in (a and b) Ar and (c and d) 5% H_2/95% Ar-purged with and without HCO_3^-/CO_3^{2-}: solid data points from Fig. 3 and 4; open data points measured prior to the XPS analyses. The full and dashed horizontal lines show the E_{CORR} values recorded in the individual run without H_2O_2.

To confirm the extent of oxidation of the electrode surface, a series of experiments was conducted in all four solutions followed by XPS analyses. In these experiments only a single H_2O_2 addition was made and the E_{CORR} was followed until it established a steady-state value. The electrode was then removed and

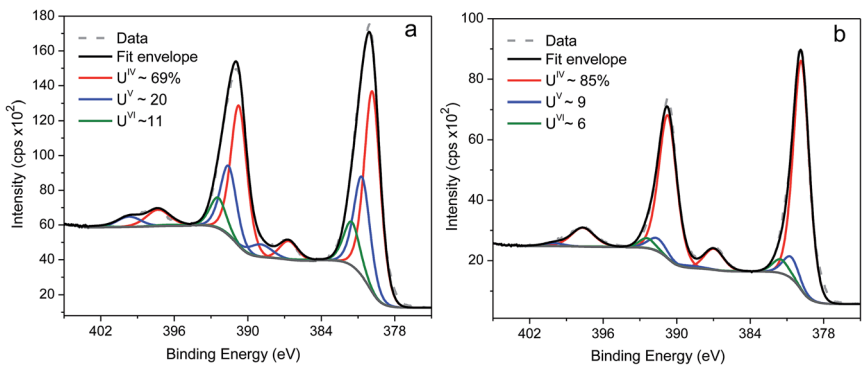

Fig. 9 XPS spectra recorded after corrosion until a steady-state E_{CORR} was achieved in a 0.1 mol L^{-1} NaCl + 5 × 10^{-2} mol L^{-1} HCO_3^-/CO_3^{2-} solution containing $[H_2O_2] \sim 8.5 \times 10^{-7}$ mol L^{-1}; (a) Ar-purged; (b) H_2/Ar-purged.

analyzed by XPS. A series of experiments was performed in each solution for different $[H_2O_2]$. Steady-state E_{CORR} values were measured twice for each solution condition to determine reproducibility, but XPS measurements were only performed on one set of measurements for each solution. These E_{CORR} values are compared to the values plotted in Fig. 7 for each experimental condition, Fig. 8, showing that, while absolute values may vary somewhat, the overall trends, as a function of $[H_2O_2]$, are consistent.

Fig. 9 shows two examples of fitted and deconvoluted XPS spectra recorded in solutions with added HCO_3^-/CO_3^{2-} containing the same $[H_2O_2]$. The less oxidized state of the surface after exposure to the H_2/Ar-purged solution (Fig. 9(b)) compared to the Ar-purged solution (Fig. 9(a)) is clear from the fractions of the individual oxidation states present in the surface.

Fig. 10 compares the atomic fractions of the oxidized states (*i.e.*, $(U^V + U^{VI})/U_{total}$) (U_{total} also contains the U^{IV} fraction) as a function of $[H_2O_2]$ for all four conditions. In the Ar-purged solutions, the fractions measured when HCO_3^-/CO_3^{2-} is present are considerably lower than those measured when no HCO_3^-/CO_3^{2-} is present. When H_2 is present the extent of surface oxidation is further suppressed, especially if HCO_3^-/CO_3^{2} is present, when significant oxidation of the surface is only observed for $[H_2O_2] \geq 10^{-5}$ mol L^{-1}.

Fig. 11 shows a plot of the atomic fraction of the oxidized states as a function of E_{CORR}, confirming that the composition of the surface dictates the value of E_{CORR} as previously proposed for similar experiments performed at higher temperatures. These observations support the claim that, when dissolved H_2 is present, the response to convection and the E_{CORR} transients, such as those shown in Fig. 4(b), can be attributed to H_2O_2-stimulated oxidation/corrosion of the $U^{IV}O_2$ surface, which can be reversed by the reaction of the surface with dissolved H_2.

This is best illustrated by revisiting the influence of added H_2O_2 on the SIMFUEL surface in an H_2/Ar-purged solution containing HCO_3^-/CO_3^{2-}, Fig. 4(b).

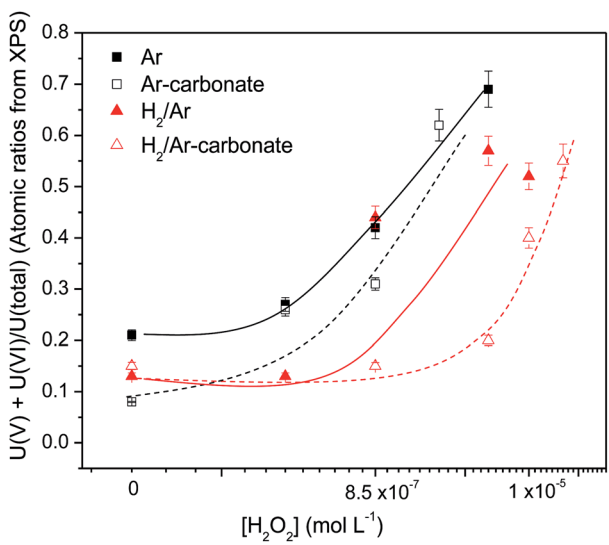

Fig. 10 The $(U^V + U^{VI})/U_{total}$ ratio as a function of $[H_2O_2]$ measured on a 1.5 at% SIMFUEL surface in Ar and 5% H_2/95% Ar-purged with and without HCO_3^-/CO_3^{2-}.

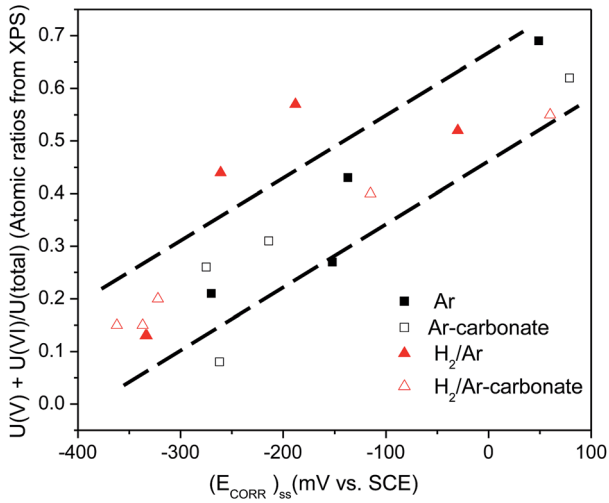

Fig. 11 Comparison of the $(U^{V} + U^{VI})/U_{total}$ ratio as a function of steady-state E_{CORR} values measured on a 1.5 at% SIMFUEL electrode at various $[H_2O_2]$ in Ar and 5% H_2/95% Ar-purged solutions with and without HCO_3^-/CO_3^{2-}.

In region 1 ($[H_2O_2] < 10^{-5}$ mol L^{-1}), oxidation of the $U^{IV}O_2$ surface is slow and, in the presence of a substantial HCO_3^-/CO_3^{2-}concentration, dissolution proceeds rapidly *via* reaction (6) with the surface remaining free of U^{VI}. In region 2, oxidation of the surface is accelerated at the higher $[H_2O_2]$, leading to the accumulation of oxidized states (U^{V}, U^{VI}) in the surface and an increase in E_{CORR}. Eventually, as depletion of the H_2O_2 proceeds, H_2 oxidation leading to matrix reduction, most likely on the galvanically-coupled ε-particles, overwhelms the matrix oxidation process. This reduction, coupled with the continuing dissolution of U^{VI} by complexation with HCO_3^-/CO_3^{2-} (reaction (6)) leads to a decrease in E_{CORR}. In region 3, when $[H_2O_2]$ is sufficiently high, an irreversible oxidation of the surface occurs, and, although not shown here, further increases in $[H_2O_2]$ have no influence on E_{CORR}.

The electrochemical oxidation of $U^{IV}O_2$ has been shown to proceed by the injection of oxygen interstitial ions (O_I^{II}) into vacant lattice positions available in the $U^{IV}O_2$ fluorite lattice, a process accompanied by, for a sufficiently low O_I^{II}, the creation of adjacent U^{V} states. Previously, we have shown, using scanning electrochemical microscopy, that this process is reversible for intermediate degrees of non-stoichiometry; *i.e.*, $x \sim 0.1$ in $U^{IV}_{1-2x}U^{V}_{2x}O_{2+x}$,[43] which adds credibility to the argument for reversibility presented here. For such a degree of non-stoichiometry, O_I^{II} can be considered to be randomly distributed within the top ~5 nm of the oxide surface, and hence extractable by reduction.

However, as the degree of non-stoichiometry increases and the composition approaches $UO_{2.25}$, cuboctahedral clusters begin to form and reversibility is lost.[43,44] As the density of such clusters increases, the lattice undergoes tetragonal distortions.[45] Although not presently demonstrated, it seems likely these distortions are a precursor to the irreversible surface oxidation, which occurs at high enough $[H_2O_2]$, see Fig. 3 and 4.

4. Summary

In terms of the overall mechanism illustrated in Fig. 2, our results confirm that reaction (2a) is reversible and that oxidation of UO_2 by H_2O_2 can be suppressed, in the presence of a sufficient concentration of dissolved H_2, by the oxidation of H_2, predominantly on ε-particles (reaction (3a)). The oxidation/dissolution (corrosion) reaction can be accelerated by the presence of HCO_3^-/CO_3^{2-} since the deposition of insulating U^{VI} corrosion products is prevented.

Under these conditions the $U^{IV}_{1-2x}U^{V}_{2x}O_{2+x}$ surface layer remains exposed to the solution, allowing the combination of reactions (2a) and (3b) to regulate the corrosion process. When exposed, this layer controls the surface redox conditions by catalyzing the decomposition of H_2O_2 to O_2 and H_2O.

For a sufficiently high $[H_2O_2]$, the UO_2 surface becomes irreversibly oxidized to the U^{VI} state. In the absence of HCO_3^-/CO_3^{2-}, this surface layer is most likely $U^{VI}O_3\cdot yH_2O$, while, when HCO_3^-/CO_3^{2-} is present, corrosion is controlled by the rate of chemical dissolution of this U^{VI} layer.

Acknowledgements

This research was funded under the Industrial Research Chair agreement between the Natural Sciences and Engineering Research Council (NSERC, Ottawa, Canada) and the Nuclear Waste Management Organization (NWMO, Toronto, Canada).

References

1 J. McMurry, D. A. Dixon, J. D. Garroni, B. M. Ikeda, S. Stroes-Gascoyne, P. Baumgartner and T. W. Melnyk, *Evolution of a Canadian Deep Geologic Repository: Base Scenario*, Ontario Power Generation Report 06819-REP-01200-10092-R00, 2003.
2 F. King and M. Kolar, *The Copper Container Corrosion Model Used in AECL's Second Case Study,* Ontario Power Generation Report 06819-REP-01200-10041-R00, 2000
3 F. King, L. Ahonen, C. Taxen, U. Vuorinen and L. Werme, *Copper Corrosion under Expected Conditions in a Deep Geologic Repository*, Swedish Nuclear Fuel and Waste Management Co, Stockholm, Sweden, TR-01-23, 2001.
4 I. Grenthe, J. Fuger, R. J. Konings, R. J. Lemire, A. B. Muller, C. Nguyen-Trung, and H. Wanne, in *Chemical Thermodynamics of Uranium*, Elsevier, Amsterdam, 1992.
5 R. Guillamont, R. T. Fanghanel, I. Grenthe, V. Neck, D. Palmer and M. H. Rand, in *Chemical Thermodynamics*, Elsevier, Amsterdam, 2003, vol. 5.
6 D. W. Shoesmith, *J. Nucl. Mater.*, 2000, **282**, 1.
7 B. G. Santos, J. J. Noel and D. W. Shoesmith, *Corros. Sci.*, 2006, **48**, 3852.
8 B. G. Santos, J. J. Noel and D. W. Shoesmith, *J. Nucl. Mater.*, 2006, **350**, 320.
9 B. G. Santos, J. J. Noël and D. W. Shoesmith, *J. Electroanal. Chem.*, 2006, **586**, 1.
10 P. G. Keech, J. S. Goldik, Z. Qin and D. W. Shoesmith, *Electrochim. Acta*, 2011, **56**, 7923.
11 I. Grenthe, F. Diego, F. Salvatore and G. Riccio, *J. Chem. Soc., Dalton Trans.*, 1984, 2439.

12 D. W. Shoesmith and F. King, Ontario Power Generation Report: 06819-REP-01200-0038R00, 1998.
13 J. S. Goldik, J. J. Noël and D. W. Shoesmith, *Electrochim. Acta*, 2006, **51**, 3278.
14 M. M. Hossain, E. Ekeroth and M. Jonsson, *J. Nucl. Mater.*, 2006, **358**, 202.
15 J. de Pablo, I. Casas, J. Gimenez, V. Marti and M. E. Torrero, *J. Nucl. Mater.*, 1996, **232**, 138.
16 J. de Pablo, I. Casas, J. Jiminez, M. Molera, M. Rovira, L. Duro and J. Bruno, *Geochim. Cosmochim. Acta*, 1999, **63**, 3097.
17 H. Kleykamp, *J. Nucl. Mater.*, 1985, **131**, 221.
18 H. Kleykamp, *Nucl. Technol.*, 1988, **80**, 412.
19 L. H. Johnson and D. W. Shoesmith, in *Spent Fuel in Radioactive Waste Forms for the Future*, ed. W. B. Lutze and R. C. Ewing, Elsevier, Amsterdam, 1988.
20 M. Razdan, M. Trummer, D. Zagidulin, M. Jonsson and D. W. Shoesmith, *Electrochim. Acta*, 2014, **130**, 29.
21 M. Razdan and D. W. Shoesmith, *J. Electrochem. Soc.*, 2014, **161**(3), H105.
22 D. W. Shoesmith, Nuclear Waste Management Organization Report TR-2007-03, 2007.
23 M. Razdan, D. Hall and D. W. Shoesmith, in *Material Research Society Symposium Proceedings*, ed. R. M. Carranza, G. S. Duffó and R. B. Rebak, Cambridge University Press, 2012, vol. 1475, p. 299.
24 M. E. Broczkowski, D. Zagidulin and D. W. Shoesmith, Nuclear Energy and the Environment, *American Chemical Society Symposium Proceedings*, 2010, vol. 1046, p. 349.
25 M. Jonsson, A. T. S. Jonsson, F. Nielsen, O. Roth, E. Ekeroth, S. Nilsson and M. M. Hossain, *Environ. Sci. Technol.*, 2007, **41**, 7087.
26 M. E. Broczkowski, J. J. Noël and D. W. Shoesmith, *J. Nucl. Mater.*, 2005, **346**, 16.
27 M. E. Broczkowski, P. G. Keech, J. J. Noël and D. W. Shoesmith, *J. Electrochem. Soc.*, 2010, **157**, C275.
28 L. Wu, Y. Beauregard, Z. Qin, S. Rohani and D. W. Shoesmith, *Corros. Sci.*, 2012, **61**, 83.
29 L. Wu, Z. Qin and D. W. Shoesmith, *Corros. Sci.*, 2014, **84**, 85.
30 L. Wu, N. Liu, Z. Qin and D. W. Shoesmith, *J. Electrochem. Soc.*, 2014, **161**, E3259.
31 P. G. Lucuta, R. A. Verrall, H. Matzke and B. J. Palmer, *J. Nucl. Mater.*, 1991, **178**, 48.
32 B. G. Santos, H. W. Nesbitt, J. J. Noel and D. W. Shoesmith, *Electrochim. Acta*, 2004, **49**, 1863.
33 M. Razdan, D. S. Hall, P. G. Keech and D. W. Shoesmith, *Electrochim. Acta*, 2012, **83**, 410.
34 M. Schindler, F. C. Hawthorne, M. S. Freund and P. C. Burns, *Geochim. Cosmochim. Acta*, 2009, **73**, 2471.
35 E. S. Ilton, J. F. Boily and P. S. Bagus, *Surf. Sci.*, 2007, **601**(4), 908.
36 M. Razdan and D. W. Shoemsith, *J. Electrochem. Soc.*, 2014, **161**, H225.
37 M. E. Broczkowski, J. J. Noel and D. W. Shoesmith, *J. Electroanal. Chem.*, 2007, **602**, 8.
38 S. Sunder, N. H. Miller and D. W. Shoesmith, *Corros. Sci.*, 2004, **46**, 1095.
39 J. C. Wren, D. W. Shoesmith and S. Sunder, *J. Electrochem. Soc.*, 2005, **152**, B470.

40 L. Wu and D. W. Shoesmith, *Electrochim. Acta*, 2014, **137**, 83.
41 L. Wu, J. S. Goldik and D. W. Shoesmith, *J. Electrochem. Soc.*, 2014, **161**, C363.41.
42 S. Nilsson and M. Jonsson, *J. Nucl. Mater.*, 2008, **374**, 290.
43 H. He, Z. Ding and D. W. Shoesmith, *Electrochem. Commun.*, 2009, **11**, 1234.
44 L. Desgranges, G. Baldinozzi, P. Simon, G. Guimbretière and A. Canizares, *J. Raman Spectrosc.*, 2012, **43**, 455.
45 H. He and D. Shoesmith, *Phys. Chem. Chem. Phys.*, 2010, **12**, 8108.